Earth and Planetary Science Letters, 110 (1992) 121–131
Elsevier Science Publishers B.V., Amsterdam

[CL]

Helium isotope geochemistry of some volcanic rocks from Saint Helena

David W. Graham [a,b,*], Susan E. Humphris [a], William J. Jenkins [a] and Mark D. Kurz [a]

[a] *Woods Hole Oceanographic Institution, Woods Hole, MA 02543, USA*
[b] *Department of Geological Sciences, University of California, Santa Barbara, CA 93106, USA*

Received May 13, 1991; revision accepted February 7, 1992

ABSTRACT

$^3He/^4He$ ratios have been measured for olivine and clinopyroxene phenocrysts in 7–15 m.y. old basaltic lavas from the island of St. Helena. Magmatic helium was effectively resolved from post-eruptive radiogenic helium by employing various extraction techniques, including *in vacuo* crushing, and stepwise heating or fusion of the powders following crushing. The inherited $^3He/^4He$ ratio at St. Helena is 4.3–5.9 R_A. Helium isotope disequilibrium is present within the phenocrysts, with lower $^3He/^4He$ upon heating and fusion of the powders following crushing, due to radiogenic ingrowth or to α-particle implantation from the surrounding (U + Th)-rich lavas.

A single crushing analysis for clinopyroxene in a basalt from Tubuaii gave $^3He/^4He = 7.1$ R_A. $^3He/^4He$ ratios at St. Helena and Tubuaii (HIMU hotspots characterized by radiogenic Pb isotope signatures) are similar to $^3He/^4He$ ratios previously measured at Tristan da Cunha and Gough Island (EM hotspots characterized by low $^{206}Pb/^{204}Pb$). Overall, the He–Sr–Pb isotope systematics at these islands are consistent with a mantle origin as contiguous, heterogeneous materials, such as recycled crust and/or lithosphere. $^3He/^4He$ ratios at HIMU hotspots are similar to mantle xenoliths which display nearly the entire range of Pb isotope compositions found at ocean islands, and are only slightly less than values found in mid-ocean ridge basalts (7–9 R_A). This suggests that the recycled materials were injected into the mantle within the last 10^9 yrs.

1. Introduction

Helium isotope studies have made a significant contribution to our understanding of mantle geochemistry. The single most important observation is that some ocean island basalts (OIB), such as those erupted at Kilauea and at Loihi Seamount in the Hawaiian island chain, on Iceland and on Réunion Island [1–8], have high $^3He/^4He$ ratios between 10–32 R_A (R_A is the atmospheric ratio of 1.39×10^{-6}). These hotspot $^3He/^4He$ ratios are higher than the relatively uniform values which characterize mid-ocean ridge basalts (MORB $^3He/^4He = 7–9$ R_A), due to a higher proportion of primordial helium, and presumably other volatiles, in the hotspot source regions. These results bear strongly on various models for the structure of the mantle and the origin of hotspots. At present, ^3He remains the only unambiguous tracer of primordial gases, and possibly of any primitive mantle material. The coupling of He isotopes to the isotope systematics of Sr, Nd and Pb provides constraints on the chemical geodynamics of the mantle.

The South Atlantic represents an important region for understanding mantle geodynamics because it contains the ocean island hotspots of St. Helena, Gough and Tristan da Cunha. Previous work has shown that Tristan da Cunha, Gough and St. Helena have $^3He/^4He$ ratios less than MORB values (with $^3He/^4He$ between approximately 4 and 6 R_A [2,9]). These results are consistent with mantle sources containing recycled crustal or lithospheric components (with elevated

Correspondence to: D.W. Graham, University of California at Santa Barbara, Department of Geological Sciences, Santa Barbara, CA 93106, USA
* Present address: College of Oceanography, Oregon State University, Corvallis, OR 97331-5503, USA

$(U + Th)/^3He$), as previously suggested from their Sr-Nd-Pb isotope and trace element compositions [2,10–18]. However, the last volcanic activity on St. Helena occurred prior to 7 m.y. ago [19–20] and the lavas are alkaline types [21–22] with high $(U + Th)/^3He$, making it difficult to identify clearly the inherited $^3He/^4He$ ratio for the island (i.e., the $^3He/^4He$ ratio of the magma at the time of eruption). A knowledge of the helium isotope signature for the mantle source of St. Helena is central to a balanced geodynamic viewpoint.

In this study we report helium, lead and strontium isotopes, and major and trace element compositions for some St. Helena lavas. We also report He isotope results for an alkali basalt from the island of Tubuaii in the South Pacific, which was previously studied for Pb, Sr and Nd isotopes. Tubuaii is characterized by radiogenic Pb isotope ratios similar to those at St Helena [23], and provides a comparative check on the generality of the St Helena helium isotope results for the so-called HIMU (high U/Pb) mantle component [15].

2. Sample locations

St. Helena, which covers an area of ~ 120 km^2, is located at 16°00′S, 5°40′W (Fig. 1). It is composed of two coalesced shield volcanoes [21–22]. The smaller northeastern volcano was mostly buried beneath the flanks of the main southwestern shield after a subaerial lifetime of approximately 3 m.y., between 14.6 and 11.4 Ma. After volcanic activity shifted to the southwest (about 12 km away) the new center continued to erupt for another 3 m.y., between 11.3 and 8.5 Ma. In the later stages, highly alkaline dikes intruded the center and upper flanks of the southwestern shield at approximately 7.5 Ma. The total subaerial lifetime was about 7 m.y. [20]. Ankaramites and picritic basalts found at stratigraphically low levels were extruded early in the history of the island, and are probably cumulative [21]. In both the northeastern and southwestern shields, basalts occur at all levels; intermediate rocks such as trachybasalts and trachytes become volumetrically more important at higher stratigraphic levels in the southwest. These were produced primarily

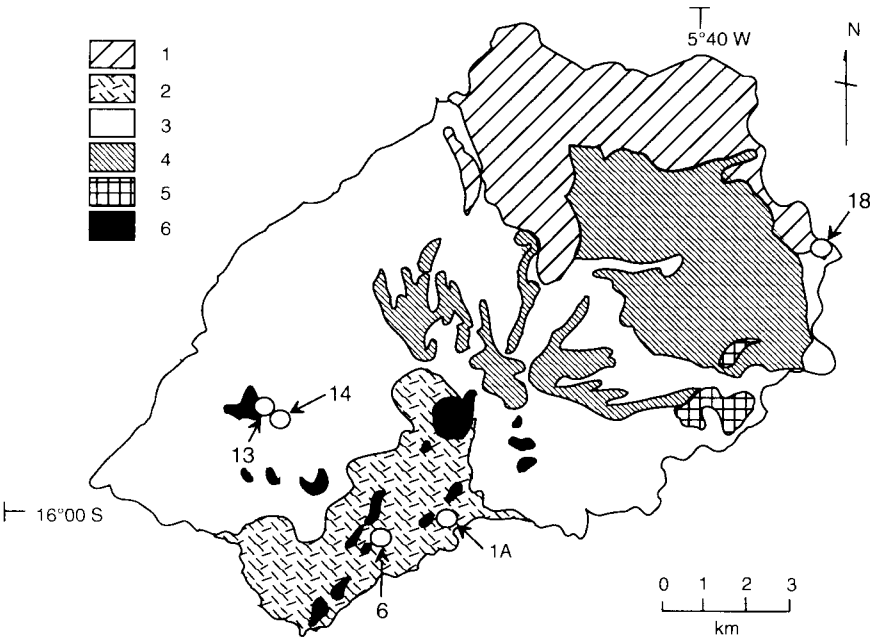

Fig. 1. Location map of St. Helena samples (after [21]). *1* = submarine and subaerial basalts of the northeastern volcano; *2* = basalt flows and pyroclastics of the lower shield; *3* = basalts and trachybasalts of the main shield; *4* = basalts and trachybasalts of the upper shield; *5* = late flank extrusives of the upper shield, including trachytes; *6* = phonolites and trachytes of the late intrusive phase.

by low-pressure differentiation, and the final phases of volcanism produced the most highly differentiated rock types. Volumetrically, basalts comprise about 70–80%, trachybasalts about 15–25%, and trachytes and phonolites < 5% [21].

Samples were collected by one of us during a cruise aboard the *Akademic Kurchatov* in 1975. Sample locations are shown in Fig. 1. Three samples representing different stages of volcanism were studied for He-Sr-Pb isotopes and chemical composition (samples CE1A, CE13 and CE18). CE1A is a porphyritic picritic basalt from a river cut near Sandy Bay, containing ~ 15% olivine + clinopyroxene phenocrysts, up to 0.8 cm in largest dimension. It is representative of the southwestern shield volcanics from 8.5–11.3 Ma. CE13 is a porphyritic alkali basalt from near High Hill, containing abundant clinopyroxene phenocrysts and minor plagioclase and altered olivine. It represents a later stage of shield volcanism. CE18 is a porphyritic ankaramite from the older (> 11.4 Ma) northeastern part of the island, near Saddle Point. It contains ~ 20% fresh clinopyroxene phenocrysts, up to 1.5 cm in size, ~ 10% highly weathered olivine, and ~ 10% vesicles which are 0.1–0.2 cm in diameter. Two additional samples (CE6, a phonolite from near Lot's Wife, and CE14, a trachybasalt from near High Hill) were also analyzed for Pb isotopes and chemical composition, but the quality and abundance of phenocrysts was insufficient for $^3He/^4He$ analysis.

3. Methods

Hand samples of rocks were cut with a diamond saw to produce subsamples having completely fresh surfaces; all saw cuts were then removed by abrasion with silicon carbide paper. Freshly cut pieces were ultrasonically cleaned in deionized water and allowed to dry before crushing in a ceramic jaw crusher. Powders for whole rock Pb and Sr analyses were prepared from these chunks using an agate ball mill. Powders analyzed for Pb were leached in cold 2 *N* HCl for 30 min, then rinsed several times with ultrapure H_2O and allowed to dry before dissolution. Pb separation and isotope analyses were performed at Lamont–Doherty Geological Observatory following procedures outlined in [9,24]. Pb blanks were ~ 1 ng during this work, and are negligible for the basalt analyses reported here. Sr analyses were performed at the University of California at Santa Barbara (UCSB) following methods described in [25]; powders analyzed for Sr were acid washed (6 *N* HCl + 7 *N* HNO_3) at 50°C for 45 min, rinsed several times with deionized water and dried prior to dissolution. Major and trace element analyses were determined by X-ray fluorescence at Woods Hole Oceanographic Institute (WHOI) following established procedures [26]. Chemical compositions and Sr-Pb isotope results are given in Table 1. The Sr and Pb isotopes, and trace element ratios (e.g., Ba/Nb) in the samples studied for He isotopes are similar to values reported previously for St. Helena lavas [10,12,17–18,22].

For helium analyses, material remaining from jaw crushing was crushed in a steel mortar, then ultrasonically cleaned several times in deionized water. Phenocrysts were hand-picked under a binocular microscope. Different phenocryst types include olivine and augite in CE1A, brown and green clinopyroxene in CE18, and augite in CE13. The green and brown pyroxenes (titanaugite and aegirine–augite, respectively) in St. Helena ankaramites have been described in [21]. Clinopyroxene in an alkali basalt from the island of Tubuaii in the South Pacific was also analyzed; Pb, Sr and Nd isotope results for this rock have been reported by Vidal et al. [23] (sample TU21; $^{206}Pb/^{204}Pb = 21.07$, $^{207}Pb/^{204}Pb = 15.76$, $^{208}Pb/^{204}Pb = 40.33$, $^{87}Sr/^{86}Sr = 0.70276$, $^{143}Nd/^{144}Nd = 0.512882$).

Helium was extracted both by crushing *in vacuo* and by fusion (1800°C) of the remaining powders in a high-vacuum, resistively-heated furnace at WHOI. Three samples were reanalyzed by crushing at UCSB, where analytical procedures and blanks were similar to those at WHOI. (At WHOI the total procedural blanks for both crushing and melting were typically $4 \pm 1 \times 10^{-11}$ ccSTP ^4He; at UCSB blanks ranged between 4 and 7×10^{-11} ccSTP ^4He. Blank corrections were usually < 10% and all reported results have been corrected accordingly. Further analytical details can be found in [8,24,27]). After crushing analysis, powders of the olivine and augite from sample CE1A were also stepwise heated in a high-temperature rock furnace (Al Forno) constructed at UCSB. The fusion and stepwise heating experi-

TABLE 1

Chemical and isotopic composition of St. Helena lavas

	CE1A	CE6	CE13	CE14	CE18
Type	pb	ph	ab	tb	ak
SiO_2	45.31	62.24	45.76	49.65	46.92
TiO_2	2.62	0.03	3.50	2.93	3.31
Al_2O_3	12.94	18.67	16.03	17.44	14.67
FeO*	12.49	3.75	12.92	11.78	12.82
MnO	0.19	0.25	0.22	0.20	0.20
MgO	11.67	0.12	5.79	3.92	6.33
CaO	10.94	0.41	10.93	7.55	10.66
Na_2O	2.05	8.14	2.57	3.63	2.45
K_2O	0.81	5.45	0.91	1.62	1.50
P_2O_5	0.49	0.02	0.30	0.77	0.47
Sum	99.51	99.08	98.93	99.49	99.33
Cr	422	< 5	68	< 5	107
Co	71	< 2	48	25	48
Ni	254	6	62	9	142
Cu	69	5	59	44	98
Rb	17	201	20	34	34
Sr	512	13	765	852	671
Y	29	63	40	65	38
Zr	211	1439	230	366	315
Nb	50	210	54	95	83
Ba	276	85	315	662	464
V	274	< 5	302	125	239
Mg#	66	7	48	41	51
$^{87}Sr/^{86}Sr$	0.702895	–	0.702877	–	0.702874
$^{206}Pb/^{204}Pb$	20.890	20.820	20.807	20.783	20.520
$^{207}Pb/^{204}Pb$	15.789	15.778	15.796	15.771	15.735
$^{208}Pb/^{204}Pb$	40.173	40.106	40.141	40.071	39.890

Oxides in weight%; trace elements in ppm. Pb isotope ratios for NBS 981 were: $^{206}Pb/^{204}Pb = 16.887 \pm 0.009$, $^{207}Pb/^{204}Pb = 15.432 \pm 0.010$, $^{208}Pb/^{204}Pb = 36.532 \pm 0.027$ (1σ, $n = 13$). All Pb data were corrected for fractionation using a 1.37‰/amu correction and are relative to standard reference values [50]. $^{87}Sr/^{86}Sr$ is normalized to 0.71025 for NBS 987. Precision ($2\sigma_{mean}$) is better than $\pm 0.05\%$/amu for Pb analyses and is better than ± 0.000012 for $^{87}Sr/^{86}Sr$. pb = picritic basalt; ph = phonolite; ab = alkali basalt; tb = trachybasalt; ak = ankaramite.

ments were designed to assess the effects of radiogenic ingrowth and α-particle implantation on the $^3He/^4He$ ratio. It was hoped that trapped and radiogenic components residing in different sites could be distinguished by sequential crushing and heating.

4. Results

He isotope results are given in Tables 2 and 3. $^3He/^4He$ ratios measured by crushing olivine and augite from CE1A (the picritic basalt from the southwestern shield) show a restricted range, between 5.0 and 5.7 R_A; He contents range between 5 and 15 nccSTP/g. Augites from CE18 (the ankaramite from the older northeastern volcano) are similar to CE1A, with $^3He/^4He = 5.9$ R_A, but with a somewhat higher He content, ~ 14–45 nccSTP/g. Augite from CE13 (the alkali basalt) has a much lower He content of 1 nccSTP/g, leading to a larger uncertainty in $^3He/^4He$ (4.3 ± 1.3 R_A).

$^3He/^4He$ ratios were also measured by melting the powders retrieved after crushing. He isotope disequilibrium exists within the phenocrysts of these old samples, with lower $^3He/^4He$ ratios upon melting in all cases. In addition, the coexisting minerals olivine and augite in CE1A have

TABLE 2

He isotope results for St. Helena and Tubuaii lavas

Sample type	Crushed				Melted Powder			
	Weight (mg)	[He] (10^{-9}ccSTP/g)	$^3He/^4He$ (R/R_A)	±	Weight (mg)	[He] (10^{-9}ccSTP/g)	$^3He/^4He$ (R/R_A)	±
St. Helena								
CE1A								
olivine 0.5–1 mm	76.5	15.1	5.73	0.27	43.8	18.2	1.54	0.28
augite 1–2 mm	83.7	10.9	5.16	0.29	41.2	103	0.15	0.06
CE13								
augite 0.5–1 mm	62.2	0.94	< 3.7					
augite*	228.1	1.40	4.25	1.25				
CE18								
augite1a 0.5–1 mm	46.2	0.53	< 7.2					
augite1b 0.5–1 mm	111.4	14.5	5.87	0.20	47.2	41.0	4.06	0.18
augite2 0.8–1 mm	99.5	45.8	5.87	0.20	56.6	113	1.38	0.06
Tubuaii								
TU 21								
cpx 0.2–0.3 mm	107.7	115	7.15	0.14	76.7	261	0.98	0.04

All analyses performed at WHOI, except * which was analyzed at UCSB.
CE 18 type 1 is aegirine augite, type 2 is titanaugite, as described in [21]; type 1a was inclusion-free. Other phenocrysts contained inclusions. Grains were selected to be free of surficial adhering matrix.

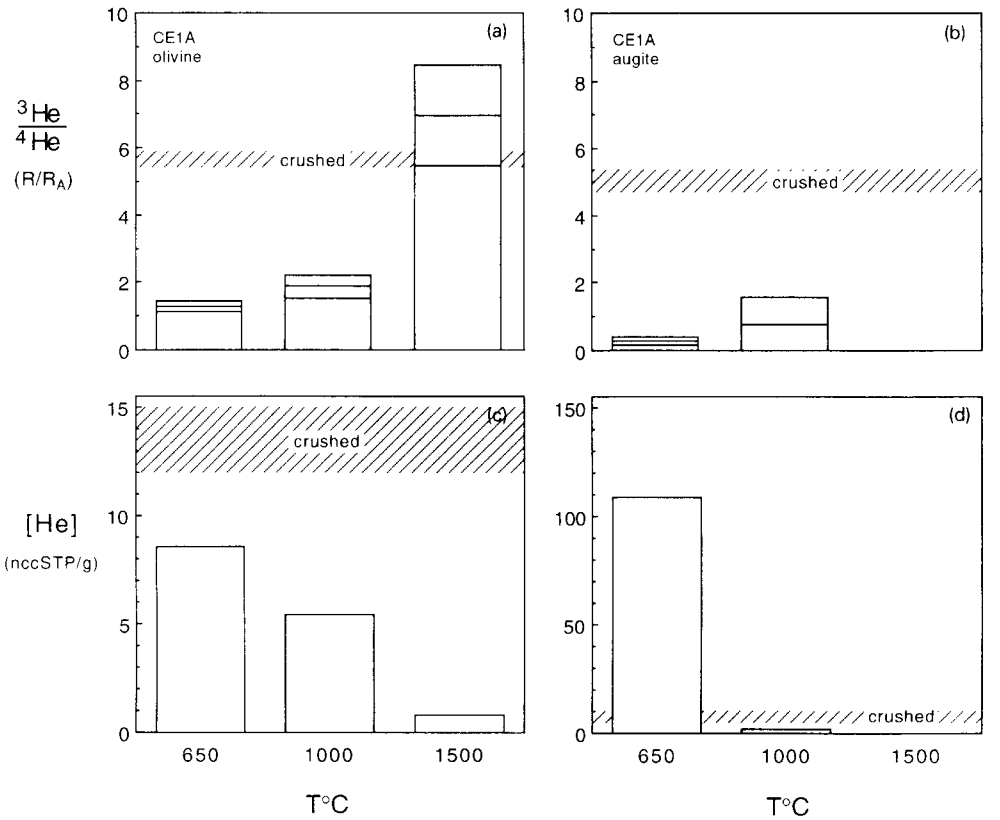

Fig. 2. Stepwise heating results for (a) and (b) olivine and (c) and (d) augite from the picritic basalt CE1A. The range of crushing results are shown for comparison. Note the difference in scales for [He] in the olivine and augite.

TABLE 3

Crushing and stepwise heating results for olivine and augite phenocrysts

Sample	Weight (mg)	T (°C)	[He] (10^{-9}ccSTP/g)	$^3He/^4He$ (R/R_A)	±
CE 1A					
olivine	182.6	crushed	12.0	5.69	0.22
	162.5	650	8.59	1.28	0.16
		1000	5.45	1.89	0.34
		1500	0.83	6.98	1.48
		total	14.9	1.81	0.30
CE 1A					
augite	192.2	crushed	5.14	5.05	0.32
	161.5	650	109	0.17	0.03
		1000	1.71	0.75	0.84
		1500	–	–	
		total	111	0.18	0.04

Stepwise heating results are for 10 min at the prescribed temperature. T was determined by optical pyrometry, and uncertainties are ±50°C. ± values are $2\sigma_{mean}$ total uncertainties, computed as the quadrature sum of precision associated with analysis of samples, standards and blanks. Blanks were determined at the relevant temperature by heating Al foil boats identical to those used to contain the sample powders. During the course of this work, furnace blanks ranged between $4–7\times10^{-11}$ ccSTP ^{4}He.

very different $^3He/^4He$ ratios and He contents upon melting (olivine with [He] = 15–18 nccSTP/g versus augite with [He] = 100–110 nccSTP/g). The augite has a $^3He/^4He = 0.15$ R_A upon melting and is clearly dominated by radiogenic ingrowth. The olivine also has a low $^3He/^4He$ ratio upon melting (1.5 R_A), but the $^3He/^4He$ ratio is above the radiogenic production ratio (~ 0.01–0.1 R_A). Despite the differences in the melting results, the "trapped" helium released by crushing gave only slightly different $^3He/^4He$ for the two phases (5.7 R_A in olivine versus 5.1 R_A in augite; Tables 2 and 3).

The cause of this slight difference in the $^3He/^4He$ ratio between helium trapped in olivine and augite for sample CE1A was further explored by stepwise heating of the powders following analysis by crushing (Table 3). Results are shown in Fig. 2. Several points are noteworthy. First, the augite released ~ 98% of its radiogenic He component at the lowest temperature step (650°C), while the olivine released < 60% of this component at the same temperature. The total amount of He released in the stepwise heating experiments (Table 3) was comparable to that released by total fusion for the respective minerals (Table 2). Secondly, the high temperature step (1500°C) gave a $^3He/^4He$ ratio for the olivine of 6.98 ± 1.48 R_A, which overlaps the ratio of 5.7 R_A obtained by crushing (the large error for the heating analysis is due to the small amount of helium released and the correspondingly larger blank correction, which was ~ 30% in this case). In contrast, the augite released all of its He below 1000°C, with $^3He/^4He$ < 1 R_A. Together these observations suggest a higher U + Th content in the augite, and possible radiation damage, or a higher degree of α-implantation from the (U + Th)-rich matrix (see below). The small difference between the crushing results for olivine (5.7 R_A) and augite (5.1 R_A) in sample CE1A can be accounted for by transfer of ~ 1% of the radiogenic component in the augite into the trapped component released by crushing. In turn, the small amount of radiogenic He released from the olivine means that its value of 5.7 R_A is the true inherited $^3He/^4He$ ratio in this St. Helena basalt.

For sample TU21 from Tubuaii, the He extracted by crushing clinopyroxene phenocrysts has a $^3He/^4He = 7.1$ R_A, slightly higher than values for St. Helena, and at the lower limit for MORB. The powder remaining from this sample was melted, yielding $^3He/^4He = 1.0$ R_A and [He] = 2.6×10^{-7} cc STP/g. Therefore, ~ 85% of the He released by melting of this sample is radiogenic, given the isotope disequilibrium observed.

5. Discussion

5.1. He isotopes in aged phenocrysts

In samples CE1A and CE18 from St. Helena, where ^3He contents released by crushing were greater than $\sim 1\times10^{-13}$ ccSTP/g, the mineral phases have similar He isotope ratios. Crushing did not release a large fraction of radiogenic He in these old (~ 1–10 m.y.) phenocrysts of relatively low (U + Th) content. This is evidence that, in favorable instances, the inherited $^3He/^4He$ ratio can be reliably estimated in old, unaltered rocks by crushing silicate phases such as olivine or pyroxene. Future studies of the inherited $^3He/^4He$ ratio of (U + Th)-poor phenocrysts may be made with reasonable confidence for some rocks as old as 10^7 m.y., and perhaps older.

U and Th concentrations have not been measured in the phenocrysts, and this is required before a He budget can be made using the stepwise heating and fusion analyses. The U content in the whole rocks can be crudely estimated from measured K_2O, assuming $K/U = 1.27 \times 10^4$ [28]. The U contents estimated in this way are ~ 0.5 and 1 ppm, respectively, for CE1A and CE18. Production of the He isotope disequilibrium in the augite of CE1A ($^3He/^4He$ of 0.15 R_A by melting as against 5.1 R_A by crushing) would require a U content of 30–40 ppb (for $Th/U = 3$; see equations in [27]). Distribution coefficients for U in clinopyroxene range from 0.002 to 0.03 [29–30]. Thus, the [U] in clinopyroxene crystallizing from a melt with ~ 1 ppm U might be as high as ~ 30 ppb, which is sufficient to support the measured [He] in the CE1A pyroxene. One might argue that most of the U and Th in these crystals resides in melt inclusions. If this is the case, values of 5.1–5.7 R_A for the trapped $^3He/^4He$ ratio suggest that crushing does not extract a significant amount of He from melt inclusions, but rather from fluid inclusion sites having low $(U + Th)/^3He$.

A complication in determining the radiogenic He component (extracted by melting) may be α-particle implantation from the surrounding rock matrix. This effect is strongly dependent upon crystal size and shape (being less significant for larger grains), upon the crystal's helium retention efficiency, and upon the distribution of U- and Th-rich accessory phases [31]. For large crystals, the amount of recoil implantation can be approximated as that for a semi-infinite slab of depth equal to the α-stopping range. Bender [32] showed that, with this simplified geometry, 25% of the α-particles generated within the α-stopping distance of the crystal surface will penetrate the crystal. At smaller grain sizes this fraction increases, because the volume over which α-particles are generated is larger relative to the crystal volume. For very small crystals the effect approximates to an isotropic case, where α-implantation equals radiogenic production in an equivalent volume of matrix, assuming efficient retention of the injected α-particles. The α-stopping distance in a basalt averages about 25 μm [9]. Approximating two crystals as spheres with diameters of 0.50 mm and 0.25 mm, surrounded by a matrix with [U] = 1 ppm, potential implantations of $\sim 1.7 \times 10^{-7}$ ccSTP/g and $\sim 3.6 \times 10^{-7}$ ccSTP/g of ^4He can occur in 10 m.y. (assuming a geometric penetration factor of 25% [32]). For the augite in sample CE1A (with a grain size of 1.5 mm, comparable to the mesh size analyzed, and with $^3He/^4He = 0.15$ R_A and an age of ~ 11.4–14.6 m.y.), α-implantation accounts for $\sim 10\%$ of the radiogenic He component. This is an upper limit because the grain size in this rock ranges up to 8 mm. Using 4 mm as the grain size, less than 1% of the radiogenic He in the augite can be attributed to α-implantation. (This effect may be underestimated somewhat for the larger sizes, because the effective surface area for the clinopyroxene grains is increased by the small fractures that are visible within the augite grains, and that probably contain minor coatings of (U + Th)-rich lava.)

The lava flow from which TU21 on Tubuaii was sampled is estimated to be 6.5–10 m.y. old [23]. A U content of 110–160 ppb (for $Th/U = 3$) could account for the amount of radiogenic He present ($\sim 2.2 \times 10^{-7}$ccSTP/g, computed from the isotope disequilibrium between crushing and melting). This clinopyroxene is fine-grained, typically 250 μm across its largest dimension. The fusion results might therefore be accounted for by α-implantation of $\sim 15\%$ of the radiogenic He generated in a surrounding lava with 1 ppm U, as outlined above.

Olivine in CE1A and augite in CE18 have inherited $^3He/^4He$ ratios of 5.8 R_A. Their similarity is significant because these two samples come from different volcanoes and, therefore, represent different stages in the petrogenetic evolution of St. Helena. Augite from the alkali basalt CE13 has a much lower trapped He content. This sample may have a slightly lower $^3He/^4He$ (4.3 ± 1.3 R_A) due to an increased dilution with radiogenic He, but the analytical uncertainties are too large to define precisely a significant difference from the other samples. Although only three St. Helena samples have been analyzed, a decrease in $^3He/^4He$ may be related to dilution by radiogenic He, from either post-eruptive or pre-eruptive (magmatic) effects. Large temporal changes in $^3He/^4He$ have been documented for Mauna Loa on a relatively short time scale of $\sim 10^4$ y [33]. At other islands, such as Réunion, the $^3He/$

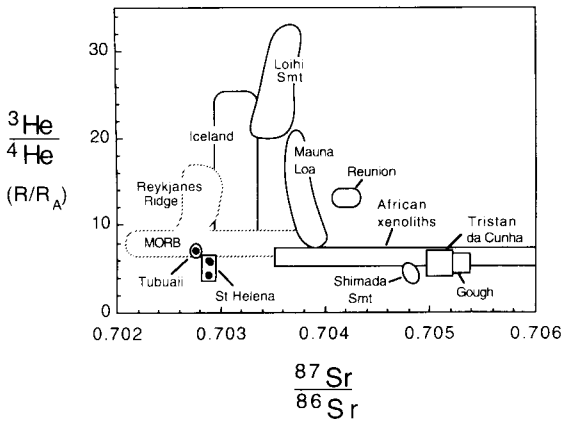

Fig. 3. $^3He/^4He$ versus $^{87}Sr/^{86}Sr$ for MORB, OIB and continental mantle xenoliths. Data sources are [2–8,24,33,42,47–49].

^4He ratio has remained constant for $\sim 10^5$–10^6 y [8]. At St. Helena, previous Pb-Sr-Nd isotope studies have suggested a slight *increase* in the HIMU component with volcanic evolution, perhaps due to a decrease in the melting of asthenospheric/lithospheric mantle, due to a decreasing thermal flux to the base of the lithosphere [22]. Temporal variations in $^3He/^4He$ may also have occurred, but we cannot address this issue with the limited data set.

5.2. Low $^3He/^4He$ signatures at hotspots

$^3He/^4He$ is shown against $^{87}Sr/^{86}Sr$ and $^{206}Pb/^{204}Pb$ in Figs. 3 and 4. Mixing of four mantle components has been suggested to account for most of the isotopic variability in OIB and MORB [14–15]. Depleted MORB mantle (DM) is characterized by non-radiogenic Pb and Sr isotope ratios and has a $^3He/^4He$ of 7–9 R_A. Other end-members are characterized by Pb-Sr-Nd isotopes similar to the sources of Walvis Ridge (termed enriched mantle, or EM1 by Zindler and Hart [15]), Sao Miguel (EM2) and St. Helena or Tubuaii (HIMU).

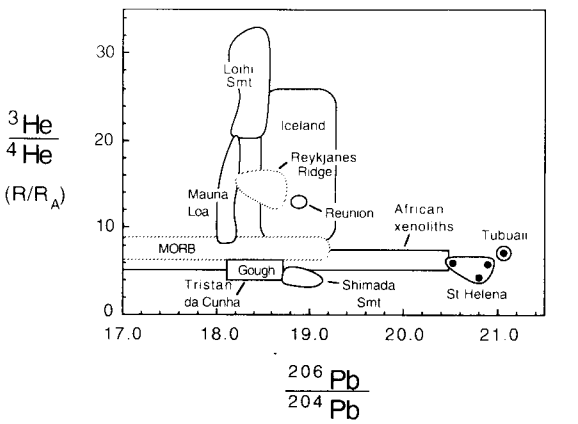

Fig. 4. $^3He/^4He$ versus $^{206}Pb/^{204}Pb$ for MORB, some OIB and mantle xenoliths. Data sources as for Fig. 3.

EM1 may be derived from recycled or metasomatized subcontinental lithosphere [13,16,34–35], or from recycled sediments [12,17–18]. In the second case, the isotopic composition of the reinjected sediments must be different from that of sediments presently being subducted beneath island arcs, and the material must have been stored in the mantle for long periods [12,17]. EM1 is not well-characterized for $^3He/^4He$. To the extent that Tristan da Cunha and Gough Island partly reflect an EM1 signature, this component may have $^3He/^4He$ ratios of ~ 4–6 R_A.

EM2 may originate from recycled sediments with compositions similar to those of the modern day, or from upper continental crust [14–15]. These materials have characteristically high $^{87}Sr/^{86}Sr$, and high $^{207}Pb/^{204}Pb$ and $^{208}Pb/^{204}Pb$ at intermediate values of $^{206}Pb/^{204}Pb$ (~ 19–20). EM2 appears to have low $^3He/^4He$ ratios (~ 3.5–5 R_A), based on He, Pb and Sr isotope results from Sao Miguel [36] and Shimada Seamount [24].

The origin of the HIMU component is less clear. Its U/Pb fractionation may result from ancient Pb removal to the lower continental crust [37] or to the Earth's core, or from recycled, altered oceanic crust [15], or from intra-mantle metasomatism by a carbonatitic fluid [38]. Based on our results, the $^3He/^4He$ ratio for the St. Helena source appears to be ~ 5.8 R_A. This value is identical to that measured in volcanic gases from Lake Nyos in western Africa [39]. These gases have a magmatic origin associated with volcanism in the Cameroon line, where some volcanic rocks also have HIMU-like Pb, Sr and Nd isotope characteristics [40]. In contrast, the value of 7.1 R_A measured for the basalt from Tubuaii suggests that the HIMU component may not be characterized by a unique $^3He/^4He$ ratio.

Both radiogenic (St. Helena type) and non-radiogenic (Tristan–Gough type) Pb isotope signa-

tures have been measured in lherzolite xenoliths from the subcontinental mantle beneath East Africa [41]. Helium in these same xenoliths displays a narrow range of $^3He/^4He$ ratios (5–7 R_A) [42], similar to the values for the South Atlantic islands (Fig. 3 and 4). Mantle xenoliths from oceanic lithosphere (< 100 m.y. old) have similar $^3He/^4He$ ratios to those from the subcontinental lithosphere (1–2 Ga old) [43]. *In situ* radiogenic production should produce different $^3He/^4He$ ratios in continental and oceanic lithosphere of such widely different ages. This homogeneity of $^3He/^4He$ may be taken as evidence that, relative to lithophile elements, helium is selectively transported into the lithosphere, and perhaps the lower crust from the upper mantle, perhaps by CO_2 or H_2O-rich fluids [43]. The xenoliths may acquire their He isotope compositions by trapping volatile-rich components which are expelled from magmas as they lose heat to conduit walls during ascent [44].

A "chronology" of mantle mixing has been proposed for some OIB hotspot sources, where homogenization of HIMU + EM1 mixtures occurs prior to mixing with a depleted mantle component [16]. This suggests that the HIMU–EM1 components have a contiguous origin, for example, as recycled lithosphere and/or lower crust [16]. According to this explanation, the wide range in Sr, Nd and Pb isotopes in continental mantle xenoliths (EM1–HIMU) reflects a long history in the subcontinental lithosphere, with variable degrees of ancient fractionation in U/Pb, Rb/Sr and Sm/Nd. In contrast, their relative homogeneity of He isotopes reflects the periodic resetting of the $(U + Th)/^3He$ system in the lithosphere and/or lower crust, prior to its recycling back into the mantle. The similar ranges of He-Sr-Pb isotopes for South Atlantic OIB and for subcontinental mantle xenoliths (Fig. 2 and 3) are consistent with a recycled origin for those OIB, as proposed earlier [2,10–13].

The "open-system" behavior of helium at the asthenosphere/lithosphere boundary may provide some constraints on the recycling time. For example, recycled ocean crust with initial [U] = 80 ppb, Th/U = 2.5, $^3He/^4He = 8\ R_A$ and [He] = 1 uccSTP/g will have $^3He/^4He \cong 5\ R_A$ after only 100 m.y. These values serve as upper limits because they are typical of unaltered MORB. The presence of sediments, or alteration of the crust prior to and during subduction will serve to increase the $(U + Th)/^3He$ ratio dramatically, and lead to a much lower $^3He/^4He$ ratio for the same time period. $^3He/^4He$ ratios of $\sim 6\ R_A$ for HIMU sources may, therefore, imply that mantle storage times for the recyled materials are relatively short (< 1 Ga).

An alternative explanation is that $^3He/^4He$ in the St. Helena source is actually lower than the values measured at the island. This would allow for possible entrainment of upper mantle material, with a MORB $^3He/^4He$ signature, during the ascent of St. Helena hotspot material. Entrainment has been shown to occur by boundary layer interactions, when thermals are produced in laboratory experiments with viscous fluids [45]. If significant entrainment of the asthenosphere occurs, the narrow range of Sr and Pb isotopes in basalts from St. Helena requires the hotspot source to have much higher Sr/He and Pb/He ratios than the entrained material. This explanation is less plausible, because He-Sr-Pb isotope relationships in South Atlantic MORB, from sections of the ridge axis where contamination by the St. Helena hotspot has been recognized, suggest that the end-member Sr/He and Pb/He ratios are not very different [46–47].

$^3He/^4He$ ratios at St. Helena indicate a mantle source with a time-integrated $(U + Th)/^3He$ which is higher than that for the MORB source. There is no evidence that the St. Helena source contains a component with high $^3He/^4He$ ratio. More work is needed on the temporal variation of $^3He/^4He$ ratios at St. Helena and other HIMU islands.

Acknowledgments

DG thanks Alan Zindler for providing facilities for the Pb isotope work at Lamont, Kaj Hoernle for performing the Sr isotope analyses at UCSB, and the Education Office at WHOI for financial assistance. John Lupton, Frank Spera, Kaj Hoernle and Jean-Guy Schilling contributed helpful discussions and encouragement and Mireille Polvé donated the Tubuaii sample. Constructive reviews by Ken Farley and Barry Hanan improved the manuscript. Helium isotope work at

WHOI was supported by OCE 85-16082 and at UCSB by OCE 88-12078 and 89-11505.

References

1 H. Craig and J.E. Lupton, Primordial neon, helium and hydrogen in oceanic basalts, Earth Planet. Sci. Lett. 31, 369–385, 1976.

2 M.D. Kurz, W.J. Jenkins and S.R. Hart, Helium-isotopic systematics of oceanic islands and mantle heterogeneity, Nature 297, 43–46, 1982.

3 M.D. Kurz, W.J. Jenkins, S.R. Hart and D. Clague, Helium isotopic variations in volcanic rocks from Loihi Seamount and the island of Hawaii, Earth Planet. Sci. Lett. 66, 388–406, 1983.

4 W. Rison and H. Craig, Helium isotopes and mantle volatiles in Loihi seamount and Hawaiian Island basalts and xenoliths, Earth Planet. Sci. Lett. 66, 407–426, 1983.

5 M. Condomines, K. Gronvold, P.J. Hooker, K. Muehlenbachs, R.K. O'Nions, N. Oskarsson and E.R. Oxburgh, Helium, oxygen, strontium and neodymium isotopic relationships in Icelandic volcanics, Earth Planet. Sci. Lett. 66, 125–136, 1983.

6 M.D. Kurz, P.S. Meyer and H. Sigurdsson, Helium isotopic systematics within the neovolcanic zones of Iceland, Earth Planet. Sci. Lett. 74, 291–305, 1985.

7 R. Poreda, J.-G. Schilling and H. Craig, Helium and hydrogen isotopes in ocean-ridge basalts north and south of Iceland, Earth Planet. Sci. Lett. 78, 1–17, 1986.

8 D. Graham, J. Lupton, F. Albarède and M. Condomines, Extreme temporal homogeneity of helium isotopes at Piton de la Fournaise, Réunion Island, Nature 347, 545–548, 1990.

9 D.W. Graham, Helium and lead isotope geochemistry of oceanic volcanic rocks from the East Pacific and South Atlantic, PhD. Dissert., Massachussetts Inst. Technol./ WHOI, 1987.

10 S.-S. Sun, Lead isotopic study of young volcanic rocks from mid-ocean ridges, ocean islands and island arcs, Philos. Trans. R. Soc. London Ser. A 297, 409–445, 1980.

11 A.W. Hofmann and W.M. White, Mantle plumes from ancient oceanic crust, Earth Planet. Sci. Lett. 57, 421–436, 1982.

12 R.S. Cohen and R.K. O'Nions, Identification of recycled continental material in the mantle from Sr, Nd and Pb isotope investigations, Earth Planet. Sci. Lett. 61, 73–84, 1982.

13 D. McKenzie and R.K. O'Nions, Mantle reservoirs and ocean island basalts, Nature 301, 229–231, 1982.

14 W.M. White, Sources of oceanic basalts: radiogenic isotopic evidence, Geology 13, 115–118, 1985.

15 A. Zindler and S.R. Hart, Chemical geodynamics, Annu. Rev. Earth Planet. Sci. 14, 493- 571, 1986.

16 S.R. Hart, D.C. Gerlach and W.M. White, A possible new Sr-Nd-Pb mantle array and consequences for mantle mixing. Geochim. Cosmochim. Acta 50, 1551–1557, 1986.

17 B.L. Weaver, D.A. Wood, J. Tarney and J.-L. Joron, Role of subducted sediments in the genesis of ocean island basalts: geochemical evidence from South Atlantic ocean islands, Geology 14, 275–278, 1986.

18 B.L. Weaver, The origin of ocean island basalt end-member compositions: trace element and isotopic constraints, Earth Planet. Sci. Lett. 104, 381–397, 1991.

19 A. Abdel-Monem and P.W. Gast, Age of volcanism on St. Helena, Earth Planet. Sci. Lett. 2, 415–418, 1967.

20 I. Baker, N.H. Gale and J. Simons, Geochronology of the Saint Helena volcanoes, Nature 215, 1451–1456, 1967.

21 I. Baker, Petrology of the volcanic rocks of Saint Helena island, South Atlantic, Geol. Soc. Am. Bull. 80, 1283–1310, 1969.

22 D.J. Chaffey, R.A. Cliff and B.M. Wilson, Characterization of the St. Helena magma source. In: Magmatism in Ocean Basins, A.D. Saunders and M.J. Norry, eds., Geol. Soc. Spec. Publ. 42, 1989.

23 P. Vidal, C. Chauvel and R. Brousse, Large mantle heterogeneity beneath French Polynesia, Nature 307, 536–538, 1984.

24 D.W. Graham, A. Zindler, M.D. Kurz, W.J. Jenkins, R. Batiza and H. Staudigel, He, Pb, Sr and Nd isotope constraints on magma genesis and mantle heterogeneity beneath young Pacific seamounts. Contrib. Miner. Petrol 99, 446–463, 1988.

25 K. Hoernle, G. Tilton and H.-U. Schmincke, Sr-Nd-Pb isotopic evolution of Gran Canaria: evidence for shallow enriched mantle beneath the Canary Islands, Earth Planet. Sci. Lett. 106, 44–63, 1991.

26 B. Schroeder, G. Thompson, M. Sulanowska and J. Ludden, Analysis of geologic materials using an automated X-ray fluorescence system, X-Ray Spectr. 9, 198–205, 1980.

27 D.W. Graham, W.J. Jenkins, M.D. Kurz and R. Batiza, Helium isotope disequilibrium and geochronology of glassy submarine basalts, Nature 326, 384–386, 1987.

28 K.P. Jochum, A.W. Hofmann, E. Ito, H.M. Seufert and W.M. White, K, U and Th in mid-ocean ridge basalt glasses and heat production, K/U and K/Rb in the mantle, Nature 306, 431–436, 1983.

29 M.G. Seitz, Uranium and thorium partitioning in diopside–melt and whitlockite–melt systems, Carnegie Inst. Wash. Yearb. 72, 581–586, 1973.

30 T. Benjamin, W.R. Heuser, D.S. Burnett and M.G. Seitz, Actinide crystal–liquid partitioning for clinopyroxene and $Ca_3(PO_4)_2$, Geochim. Cosmochim. Acta 44, 1251–1264, 1980.

31 D.J. Martel, R.K. O'Nions, D.R. Hilton and E.R. Oxburgh, The role of element distribution in production and release of radiogenic helium: the Carnmellis Granite, southwest England, Chem. Geol. 88, 207–221, 1990.

32 M.L. Bender, Helium–uranium dating of corals, PhD. Diss., Columbia Univ., 1970.

33 M.D. Kurz and D.P. Kammer, Isotopic evolution of Mauna Loa volcano, Earth Planet. Sci. Lett. 103, 257–269, 1991.

34 S.H. Richardson, A.J. Erlank, A.R. Duncan and D.L. Reid, Correlated Nd, Sr and Pb isotope variation in Walvis Ridge basalts and implications for evolution of their mantle source, Earth. Planet. Sci. Lett. 59, 327–352, 1982.

35 C.J. Hawkesworth, M.S. M. Mantovani, P.N. Taylor and Z. Palacz, Evidence from the Parana of south Brazil for a

continental contribution to Dupal basalts, Nature 322, 356–358, 1986.
36 M.D. Kurz, R.B. Moore, D.P. Kammer and A. Gulesserian, An isotopic study of dated alkali basalts from Sao Miguel, Azores: implications for the origin of the Azores hotspot, Earth Planet. Sci. Lett., in press.
37 H.E. Newsom, W.M. White, K.P. Jochum and A.W. Hofmann, Siderophile and chalcophile element abundances in oceanic basalts, Pb isotope evolution and growth of the Earth's core, Earth. Planet. Sci. Lett. 80, 229–313, 1986.
38 M. Tatsumoto, D.M. Unruh, P. Stille and H. Fujimaki, Pb, Sr and Nd isotopes in oceanic island basalts, Proc. Int. Geol. Congr., 27th, Vol. 2, Geochemistry and Cosmochemistry, pp. 485–501, 1984.
39 Y. Sano, M. Kusakabe, J. Hirabayashi, Y. Nojiri, H. Shinohara, T. Njine and G. Tanyileke, Helium and carbon fluxes in Lake Nyos, Cameroon: constraint on next gas burst, Earth Planet. Sci. Lett. 99, 303–314, 1990.
40 A.N. Halliday, J.P. Davidson, P. Holden, C. DeWolf, D.-C. Lee and G. Fitton, Trace-element fractionation in plumes and the origin of HIMU mantle beneath the Cameroon line, Nature 347, 523–528, 1990.
41 R.S. Cohen, R.K. O'Nions and J.B. Dawson, Isotope geochemistry of xenoliths from East Africa: implications for development of mantle reservoirs and their interaction, Earth Planet. Sci. Lett. 68, 209–220, 1984.
42 D.R. Porcelli, R.K. O'Nions and S.Y. O'Reilly, Helium and strontium isotopes in ultramafic xenoliths, Chem. Geol. 54, 237–249, 1986.
43 D. Vance, J.O. H. Stone and R.K. O'Nions, He, Sr and Nd isotopes in xenoliths from Hawaii and other oceanic islands, Earth Planet. Sci. Lett. 96, 147–160, 1989.
44 F.J. Spera, Dynamics of translithospheric migration of metasomatic fluid and alkaline magma, in: Mantle Metasomatism, M.A. Menzies and C.J. Hawkesworth, eds., pp. 1–20, Academic Press, New York, 1987.
45 R.W. Griffiths, The differing effects of compositional and thermal buoyancies on the evolution of mantle diapirs, Phys. Earth Planet. Inter. 43, 261–273, 1986.
46 B.B. Hanan, R.H. Kingsley and J.-G. Schilling, Pb isotope evidence in the South Atlantic for migrating ridge-hotspot interactions, Nature 322, 137–144, 1986.
47 D.W. Graham, W.J. Jenkins, J.-G. Schilling, G. Thompson, M.D. Kurz and S.E. Humphris, Helium isotope geochemistry of mid-ocean ridge basalts from the South Atlantic, Earth Planet. Sci. Lett., in press, 1992.
48 M.D. Kurz, W.J. Jenkins, S.R. Hart and J.-G. Schilling, Helium isotopic variations in the mantle beneath the central North Atlantic Ocean, Earth Planet. Sci. Lett. 58, 1–14, 1982.
49 J.J. Mahoney, J.H. Natland, W.M. White, R. Poreda, S.H. Bloomer, R.L. Fisher and A.N. Baxter, Isotopic and geochemical provinces of the western Indian Ocean spreading centers, J. Geophys. Res. 94, 4033–4052, 1989.
50 E.J. Catanzaro, T.J. Murphy, W.R. Shields and E.L. Garner, Absolute isotopic abundance ratios of common, equal-atom, and radiogenic lead isotopic standards. J. Res. Natl. Bur. Stand. 72A, 1968.